Available online at www.sciencedirect.com
SCIENCE DIRECT
Journal of Power Sources 157 (2006) 592–599
JOURNAL OF POWER SOURCES
www.elsevier.com/locate/jpowsour

Thermal analysis of rapid charging nickel/metal hydride batteries

Jianzhen Shi, Feng Wu *, Shi Chen, Cunzhong Zhang

School of Chemical Engineering and Environment, Beijing Institute of Technology, Beijing 100081, China

Received 23 June 2005; received in revised form 31 July 2005; accepted 4 August 2005
Available online 25 October 2005

Abstract

A two-dimensional thermal model was presented to predict the temperature distribution of cylindrical 8-Ah Ni/MH battery. Under the forced convection, the temperature rise of the battery is up to about 37, 42 and 51 °C, and the temperature profiles become non-uniformed at the end of 1*C*, 2*C* and 4*C* rate charge, respectively. It is indicated that the increase of the convection coefficient can decrease the battery temperature, however, lead seriously to the less uniform temperature profile across the battery. The numerical studies indicate that the increase of thermal conductivity can improve the uniformity of temperature profile to some extends. The battery temperature increases obviously when charged at higher rates. Overcharge can result in an increasingly higher temperature rise and a steeper temperature gradient within a battery.

Keywords: Thermal modeling; Ni/MH battery; Temperature gradient

1. Introduction

The spirally wound design is generally employed in the manufacture of cylindrical Ni/MH battery. This design is of importance to battery in the improvement of the energy and power densities because of its lesser accessories when compared with the prismatic design [1], therefore, it is widely adopted in the batteries for hybrid electrical vehicles (HEV) emphasizing high specific power. However, the specific area is smaller for the spiral design, and the cylindrical batteries retain more heat and less uninformed temperature profiles under the larger loads, seriously leading to the performance fade in the case of the high power batteries for HEVs. Battery failure could also result from excessive temperature rise and steeper temperature gradient within a battery [2]. So it is important to study heat transport in the batteries.

Fast charge is technically needed in the case of batteries for HEV applications. There exist lots of challenges because of difficulties in controlling the charging protocols under dynamic conditions during fast charge. Thermal control is one of the challenges for fast charge. Modeling and simulation of batteries are useful methods for studying and developing the rapid charging process [3]. Thermal modeling based on the first principles is capable of providing valuable internal information to help optimize the battery system in a cost-effective manner [4]. Mathematical simulation of thermal transport within batteries is an effective tool to obtain the knowledge about whether excessive heat generated during the battery discharge/charge process can be removed and how the operating temperature can be controlled [5]. This has been done for some cylindrical batteries—Li/$SOCl_2$ battery [6] and Li/BCX system [7]. Based on an assumption of uniformed temperature profile across the whole battery, coupled thermal/electrochemical models were proposed to investigate a larger prismatic and a small commercial nickel/metal hydride battery, respectively [3,4]. A two-dimensional thermal model with a constant rate of heat generation has been presented to analyze a 30 and a 16 Ah prismatic nickel/metal hydride battery and packs [8,9]. In the case of cylindrical Ni/MH batteries used for HEVs, however, there exist few publications in which present theoretical analyses of thermal investigation. In the present work, a two-dimensional math-

* Corresponding author. Tel.: +86 10 68912657; fax: +86 10 68451429.
E-mail addresses: stonesjz@vip.163.com, wufeng863@vip.sina.com (F. Wu).

0378-7753/$ – see front matter © 2005 Elsevier B.V. All rights reserved.
doi:10.1016/j.jpowsour.2005.08.005

Nomenclature

A	the area for dissipating heat (m^2)
$C_{battery}$	nominal capacity (Ah)
C_p	heat capacity ($J\,kg^{-1}\,K^{-1}$)
$C_{p,ref}$	reference heat capacity ($J\,kg^{-1}\,K^{-1}$)
h	convection heat-transfer coefficient ($W\,m^{-2}\,K^{-1}$)
H	battery height (mm)
i	current (A)
l_c	thickness of the case wall (mm)
L	total thickness of a battery (mm)
m	as defined in Eq. (12)
M	mass of battery (kg)
q	heat generation rate per unit volume ($J\,m^{-3}\,s^{-1}$)
Q	heat generation rate ($J\,s^{-1}$)
r	direction perpendicular to electrodes
R_d	internal resistance (Ω)
R	battery radius (mm)
t	time (s)
T	temperature of battery (°C)
T_∞	ambient temperature (°C)
T_0	initial temperature (°C)
T_{ref}	reference temperature (°C)
U	battery voltage (V)
U_0	open-circuit potential
V	battery volume (m^3)
z	direction parallel to electrodes
δ_p	the volume fraction of positive electrode
δ_s	the volume fraction of separator
δ_n	the volume fraction of negative electrode
ε	porosity (%)
θ	state-of-charge
λ_c	thermal conductivity of wall ($W\,m^{-1}\,K^{-1}$)
λ_n	thermal conductivity of negative electrode ($W\,m^{-1}\,K^{-1}$)
λ_p	thermal conductivity of positive electrode ($W\,m^{-1}\,K^{-1}$)
λ_s	thermal conductivity of separator ($W\,m^{-1}\,K^{-1}$)
λ_r	thermal conductivity in the r-direction ($W\,m^{-1}\,K^{-1}$)
λ_z	thermal conductivity in the z-direction ($W\,m^{-1}\,K^{-1}$)
ρ	average density ($kg\,m^{-3}$)

ematical model containing temporal and spatial coordinates, with variable heat generation rates and temperature gradients across the battery, was presented for analyzing the thermal behavior and obtaining the internal temperature profile of cylindrical Ni/MH battery with different design and operational conditions.

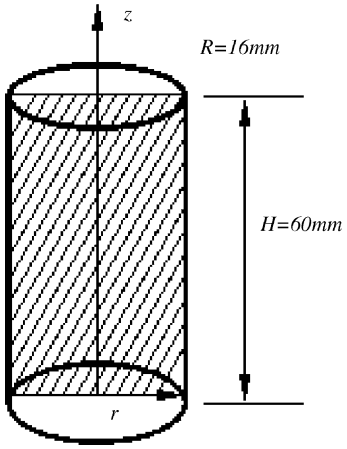

Fig. 1. Schematic diagram of a cylindrical 8-Ah Ni/MH battery.

2. Model description

The cylindrical Ni/MH battery (as Fig. 1) is composed of a porous positive electrode, a separator, and a negative electrode, which were spirally wound and inserted into a stainless steel case.

In general, a thermal model is formulated based on the thermal energy balance over a representative elementary volume in a battery. For most battery systems, the convection term can generally be neglected. The following transient partial differential equation Eq. (1) is sufficient to describe the temperature profile in the cylindrical battery under the conditions of angular symmetry when the temperature gradients and the heat fluxes are zero in the angular direction [4,5]

$$\rho\frac{\partial(C_pT)}{\partial t} = \frac{1}{r}\frac{\partial}{\partial r}\left(r\lambda_r\frac{\partial T}{\partial r}\right) + \frac{\partial}{\partial z}\left(\lambda_z\frac{\partial T}{\partial z}\right) + q \tag{1}$$

where T is the temperature, q the volumetric heat generation rate, ρ represents the volume averaged density, C_p denotes the specific heat, δ_r and δ_z are the heat conductivities of r-direction and z-direction, respectively. For simplicity, according to the assumption of Bernard et al. [10], the heat generation rate is assumed to be distributed uniformly throughout the battery using the volume-averaging approach under the assumption that no phase change is involved and only electrochemical/intercalation reactions exist for the Ni/MH battery of the present investigation, hence, heat generation rate can be written as

$$q = \frac{i}{V}\left[(U - U_0) - T\frac{dU_0}{dT}\right] \tag{2}$$

where i represents the current, V the battery volume, U denotes the battery voltage, U_0 is the open-circuit potential of a battery. The heat generation rate generally consists of the joule heat $i(U - U_0)$ (irreversible) and the reversible heat effect ($iT\,dU_0/dT$). Heat conductivities are considered as constants in the thermal model for simplicity. According to Ref. [1], the battery temperature coefficient (dU_0/dT) of the bat-

tery is presented as

$$\frac{dU_0}{dT} = \frac{dU_{p,0}}{dT} - \frac{dU_{n,0}}{dT} \quad (3)$$

where the first term on the right side denotes the positive electrode temperature coefficient, the second term represents the negative electrode temperature coefficient.

When a battery was overcharged, q consists of the joule heat and the oxygen recombinant heat at the hydride electrode, according to Ref. [11].

$$q = 1.48i + R_d i \quad (4)$$

The first term denotes the oxygen recombinant heat at the hydride electrode, and the second term arises from ohmic heat from the battery internal resistance R_d, which is assumed to constantly be 3 mΩ according to our measurement in this work.

It is further assumed that the radiation conduction from the battery to the ambient is neglected and only cooling by convection is significant at the boundary, and Newton's cooling law is applied to boundary conditions. So the boundary and initial conditions can be written as follows,

$$-\lambda_r \frac{\partial T}{\partial r} = \left(\frac{1}{h} + \frac{l_c}{\lambda_c}\right)^{-1} (T - T_\infty) \quad \text{at } r = R \quad (5)$$

$$-\lambda_r \frac{\partial T}{\partial r} = 0 \quad \text{at } r = 0 \quad (6)$$

$$\lambda_z \frac{\partial T}{\partial z} = \left(\frac{1}{h} + \frac{l_c}{\lambda_c}\right)^{-1} (T - T_\infty) \quad \text{at } z = 0 \quad (7)$$

$$-\lambda_z \frac{\partial T}{\partial z} = \left(\frac{1}{h} + \frac{l_c}{\lambda_c}\right)^{-1} (T - T_\infty) \quad \text{at } z = H \quad (8)$$

$$T = T_0 \quad \text{at } t = 0 \quad (9)$$

where l_c is the thickness of the steel case wall, λ_c the heat conductivity of the case wall; T_∞ the ambient temperature, and h is the thermal transfer coefficient.

The above boundary conditions imply that the core of the spiral is adiabatic, while the outer boundary exchanges heat with the ambience through a heat-transfer coefficient h. The spiral is set at a uniform initial temperature T_0 to which the ambient temperature equals.

Table 1
Parameters for thermal model calculation

Parameters	Values
Battery radius (mm), R	16
Battery height (mm), H	60
Battery density (kg m^{-3}), ρ	3900
Initial temperature (°C), T_0	24.4
Thickness of case wall (mm), l_c	5
Heat conductivity of case wall (W m^{-1} K^{-1}), λ_c	468
Positive electrode temperature coefficient (V K^{-1}), $dU_{p,0}/dT$	-1.0×10^{-3} [3]
Negative electrode temperature coefficient (V K^{-1}), $dU_{n,0}/dT$	-6.3×10^{-4} [3]

Table 2
Average heat conductivities of battery components

	Negative electrode	Positive electrode	Separator
λ_m (W m^{-1} K^{-1})	1.16[a]	1.14[a]	0.22[b]
$\varepsilon_{(porosity)}$	0.25[c]	0.30[c]	0.74[a]
λ_f (W m^{-1} K^{-1})	0.57[d]	0.57[d]	0.57[d]
$\delta_{i(fraction)}$	0.29	0.45	0.27
λ_I (W m^{-1} K^{-1})	1.01[e]	0.97[e]	0.48[e]

[a] Ref. [9].
[b] Ref. [14].
[c] Measured results.
[d] Ref. [15].
[e] The average thermal conductivities of each component are estimated by Ref. [15].

The parameters used in the thermal modeling of the cylindrical Ni/MH battery are listed in Tables 1 and 2.

3. Experimental details

Cylindrical 8-Ah Ni/MH batteries fabricated in our laboratory were adopted to test the temperature distribution during charge and discharge. An 8-Ah cylindrical Ni/MH battery was constructed by winding a positive electrode and a negative electrode and a porous polypropylene separator switched in between the electrodes. The case encasing the electrode groups is made of stainless steel with a thickness of 0.5 mm. β-Ni(OH)$_2$ is active material of positive electrode, AB_5 alloy powder as active material of negative electrode, consists of $MmNi_{3.75}Co_{0.55}Al_{0.3}Mn_{0.4}$. KOH solution (30 wt%) acted as electrolyte in this work. The battery parameters are listed in Table 1.

Arbin BT Cycler was used to control the process of charging under the constant current condition. Thermocouples were used to measure the temperature changes on the battery surface. The data of current, voltage and temperature were recorded by Arbin BT Cycler.

In order to estimate the unknown heat capacity, smaller size AA 1.8 Ah cylindrical Ni/MH batteries with the same chemistry and design were measured to test the temperature and voltage curves during the relaxation period. The advantage choosing small batteries is that their Biot number [12] can be so small that there are no significant temperature profiles inside the batteries under the normal operating conditions.

4. Results and discussion

4.1. Estimation of heat capacity

To estimate the actual heat capacity, a small cylindrical AA 1.8-Ah Ni/MH battery with the same chemistry and design was charged at 1C, 2C, 4C rates separately. Since there is no significant temperature profile inside the small battery because of the small Biot number [12] under the condition given by Eq. (10), the assumption of a uniform temperature

profile across the small battery is valid and hence a lump-parameter model of energy balance can be applied. The heat energy equation (Eq. (1)) is thus reduced to Eq. (11),

$$Bi = \frac{hL}{\lambda} \ll 1 \tag{10}$$

where h is the free-convective heat-transfer coefficient, L represents the thickness of battery, respectively

$$M\frac{\mathrm{d}(C_\mathrm{p}T)}{\mathrm{d}t} = Ah(T_\infty - T) + Q \tag{11}$$

where M denotes the mass of battery, A the surface area through which heat is removed from the battery and Q is the heat generation rate in watts.

C_p is a function of temperature by fitting the temperature–time curves during the relaxation periods, and C_p is treated to be varied linearly with temperature as given by

$$C_\mathrm{p} = C_{\mathrm{p,ref}}[1 + m(T - T_\mathrm{ref})] \tag{12}$$

Where $C_{\mathrm{p,ref}}$ is the reference heat capacity when the temperature equals T_ref.

Substituting Eq. (12) into Eq. (11), Eq. (13) can then be obtained when the current is turned off after charging finished [13], i.e. $Q = 0$.

$$\frac{hA}{MC_{p,\mathrm{ref}}}t = (1 + mT_\infty)\ln\left(\frac{T_0 - T_\infty}{T - T_\infty}\right) + 2m(T_0 - T) \tag{13}$$

C_p and m can be obtained by fitting the temperature–time curves as Eq. (13) measured during the relaxation periods following charge. From Fig. 2, $C_{\mathrm{p,ref}}$ and m values were obtained, $C_{\mathrm{p,ref}} = 1882\ \mathrm{J\,kg^{-1}\,K^{-1}}$ and $m = -0.001$.

4.2. Estimation of heat conductivities

The heat conductivities λ_r and λ_z as constants are highly anisotropic and microstructure-dependent and are estimated according to the following equations [5],

$$\text{series-connected } \frac{1}{\lambda_r} = \sum_i \frac{\delta_i}{\lambda_i} = \frac{\delta_\mathrm{p}}{\lambda_\mathrm{p}} + \frac{\delta_\mathrm{s}}{\lambda_\mathrm{s}} + \frac{\delta_\mathrm{n}}{\lambda_\mathrm{n}} \tag{14}$$

$$\text{Parallel-connected } \lambda_z = \sum_i \delta_i\lambda_i = \delta_\mathrm{p}\lambda_\mathrm{p} + \delta_\mathrm{s}\lambda_\mathrm{s} + \delta_\mathrm{n}\lambda_\mathrm{n} \tag{15}$$

Where δ_p, δ_s and δ_n denote the volume fractions of the positive electrode, the separator and the negative electrode, respectively; λ_p, λ_s and λ_n represent the average heat conductivities of positive electrode, separator and negative electrode, respectively. Table 2 summarizes the average heat conductivities of battery components. According to Table 2, Eqs. (14) and (15), λ_r and λ_z are estimated to be 0.74 and $0.85\ \mathrm{W\,m^{-1}\,K^{-1}}$, respectively, Ref. [9].

$$\lambda_i = \lambda_\mathrm{m}(1 - \varepsilon) + \lambda_\mathrm{f}\varepsilon \tag{16}$$

Where ε is porosity, λ_m and λ_f are the heat conductivities of structural materials and filling electrolyte materials, respectively.

4.3. The average surface temperature profiles

FEMLAB®, a commercial FEA software system, is employed to solve the heat equations in this work. Fig. 3 shows the charging curves of 8-Ah Ni/MH battery at 1C, 2C and 4C rates, respectively. The voltage curves are then fitted to calculate the joule heat in Eq. (1). Open circuit voltage (OCV) can be written as a function of state-of-charge (θ) denoting the average battery state-of-charge defined to be

$$\theta = \frac{it}{C_\mathrm{battery}} \tag{17}$$

where t is the time in hours, and C_battery is the battery nominal capacity.

The calculated and measured average surface temperature profiles were compared in Fig. 4 at varying charging times

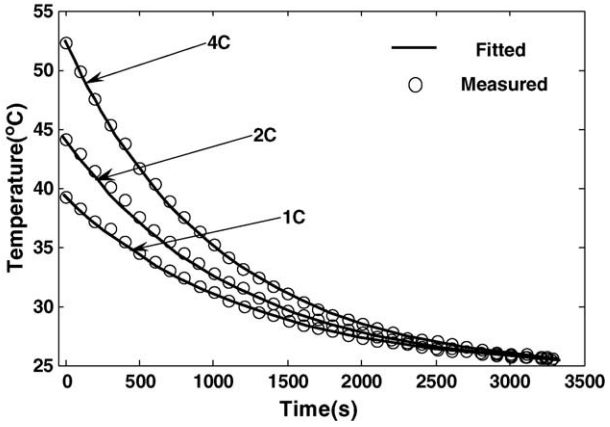

Fig. 2. Estimation of the C_p and m by fitting the measured values during the relaxation periods.

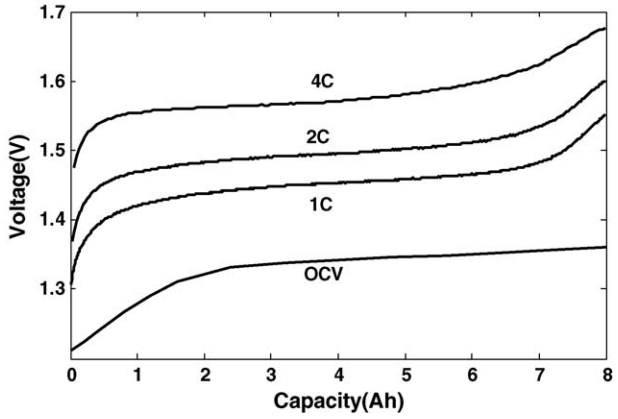

Fig. 3. Charging curves of an 8-Ah cylindrical Ni/MH battery during 1C, 2C and 4C constant current charge.

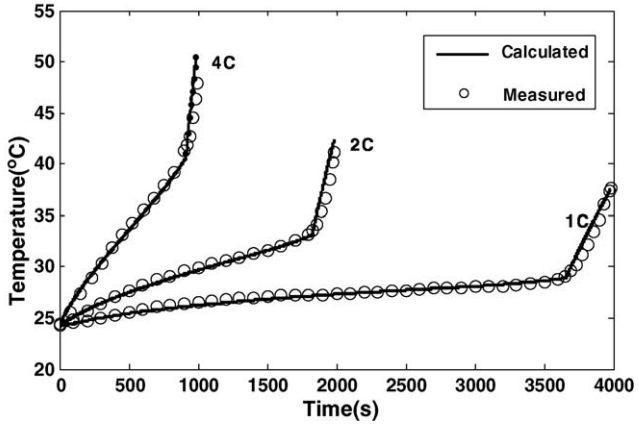

Fig. 4. The measured and calculated average surface temperature variations of the battery during charge at 1*C*, 2*C* and 4*C* constant current under forced convection ($h = 25\ \mathrm{W\,m^{-2}\,K}$).

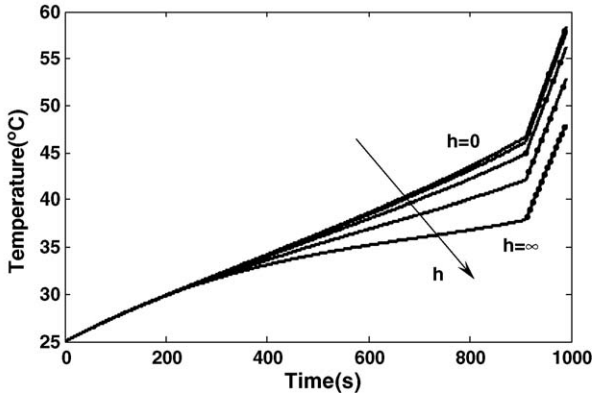

Fig. 5. Calculated temperature rise in the centre of a battery with different heat-transfer coefficients ($h = 0$, 6, 25, 100, ∞, $\mathrm{W\,m^{-2}\,K^{-1}}$).

under the forced convection ($h = 25\ \mathrm{W\,m^{-2}\,K^{-1}}$). The steeper parts of three cures mean overcharge. The average surface temperature rises from 24.4 to 29, 33 and 41 °C at the end of 1*C*, 2*C* and 4*C* charge, respectively, when the imputed charge equals 110% of nominal capacity, the average surface temperature rises rapidly to 37, 42 and 51 °C at 1*C*, 2*C* and 4*C* overcharge, respectively. It is showed that the average surface temperature increases when the charging rates increase. The battery temperature increase with time under all cases, indicating that the battery is exothermic during charge. When the battery was charged at a rate as large as 4*C*, the calculated temperature is slightly lower than the measured values before 100% capacity. This is probably own to a low estimation of the oxygen recombinant heat which is highly larger than the ohmic heat, because the oxygen reaction current increases and the primary reaction current decreases when charged at higher rates. The results from the simulation are well in agreement with experimental measurements at the range from 1*C*, 2*C* to 4*C* charge in spite of a slight higher predicted value during the overcharge. The rate of heat generation was overestimated during overcharge in Eq. (4). It is because that the oxygen generated at the positive electrode was not entirely reduced at the negative electrode, but only a portion of oxygen was reduced under a higher battery internal pressure, therefore, the oxygen recombinant heat is not so much as that in Eq. (4).

4.4. Effect of heat-transfer coefficients on temperature distribution

Fig. 5 compares the predicted temperature distributions in the centre of the battery under free, forced convection and adiabatic conditions. Five thermal conditions were considered in terms of an equivalent heat-transfer coefficient imposed on the surface. Where $h = 0$ and $h = \infty$ correspond to adiabatic and isothermal conditions, respectively, $h = 6$ and $25\ \mathrm{W\,m^{-2}\,K^{-1}}$ refer to typical values of air-free convection and forced convection, $h = 100\ \mathrm{W\,m^{-2}\,K^{-1}}$ represents the extended forced convection.

It is indicated that the battery temperature is remarkably lower under forced convection than free convection. This discrepancy is ascribed to the fact that forced convection can sufficiently dissipate the generated heat. The adiabatic behavior was also investigated with the assumption of the same charging characteristics; temperature rise under the adiabatic condition is significantly higher than those under the convection condition. Adiabatic modeling is important because we must consider the consequences of no heat removal, for example, the accident if the temperature-control system fails. Under the adiabatic condition, the temperature increases up to about 47 °C at 100% charge input, and dramatically up to about 60 °C at 110% charge input, it is obvious that adiabatic charge is highly dangerous. As the heat-transfer coefficients increase, the temperature in the centre of battery is prone to a lower value, when the heat-transfer coefficients increase close to infinite, which means the temperature on the surface of case wall was constantly kept close to the initial temperature, the temperature in the centre of battery is about 10 °C lower when compared with the adiabatic condition. A larger heat-transfer coefficient corresponds to a larger rate of heat dissipation, resulting in a smaller temperature rise during battery charging. When the heat transfer coefficient is equal to $6\ \mathrm{W\,m^{-2}\,K^{-1}}$, the battery centre temperature rises up to 58 °C at 110% of the nominal battery capacity. As the heat-transfer coefficient increases ($25\ \mathrm{W\,m^{-2}\,K^{-1}}$), the final battery temperature decreases. The calculated results indicate increasing heat transfer coefficient can decrease the centre temperature which is the maximum temperature inside the whole battery. A lower temperature can be obtained at a higher heat dissipation rate.

Fig. 6 is a two-dimensional temperature profile in the *r*- and *z*-directions under the free (A) and forced convection (B) at the end of 4*C* charge (110% of nominal capacity). It can be seen that the average temperature of the battery is strongly affected by cooling conditions. The higher the heat dissipation rate, the lower the battery temperature. It also

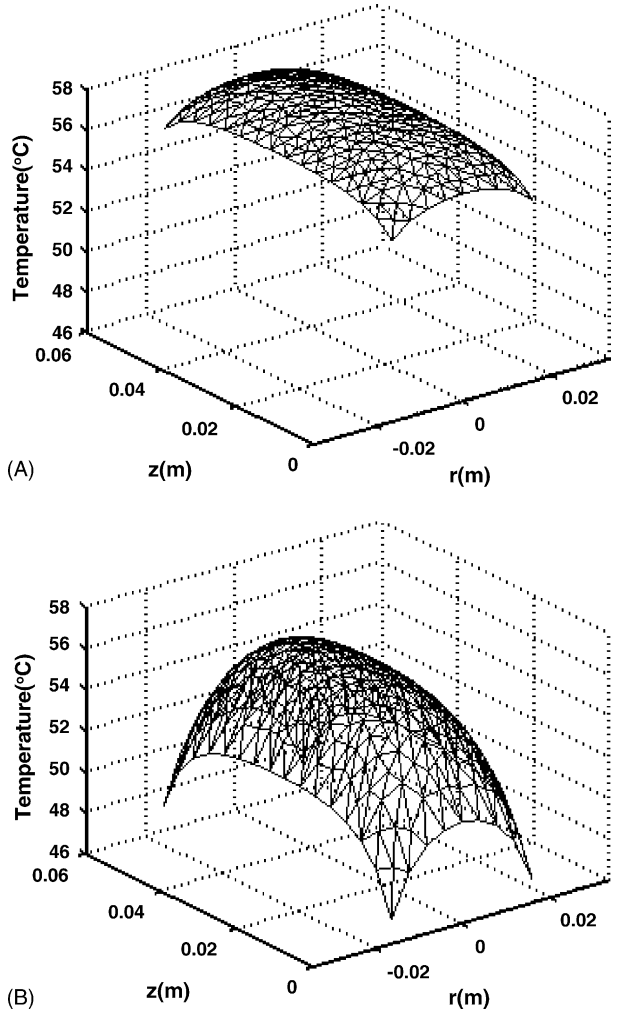

Fig. 6. Temperature profiles in r- and z-direction at the end of 4C charge (A: $h = 6$; B: $h = 25$, $T_0 = 25\,^{\circ}C$).

reveals that the temperature distribution at the end of charge become more non-uniformed across the battery especially in r-direction, because the heat is transferred faster at the side of battery compared to that in the centre of battery when heat-transfer coefficient increases. Although the temperature decreases remarkably with a higher heat-transfer coefficient, the temperature profile across the battery become more non-uniformed, it is clearer in Fig. 7. Obviously, in order to prevent the significant increase of the temperature in the battery under higher charge rates, the improvement in cooling conditions is necessary; however, it is not helpful to uniformity of temperature profile across the battery. Instead, it may cause steeper temperature profiles. The large temperature gradients in r-direction may suggest that the low conductivity in r-direction will limit heat removal rate, and therefore the heat transport behavior in the battery is mainly characterized by the low thermal conductivity of separator.

Fig. 7 depicted the effect of different heat-transfer coefficient on the difference between maximum and minimum temperature obtained from the thermal model for 4C charge.

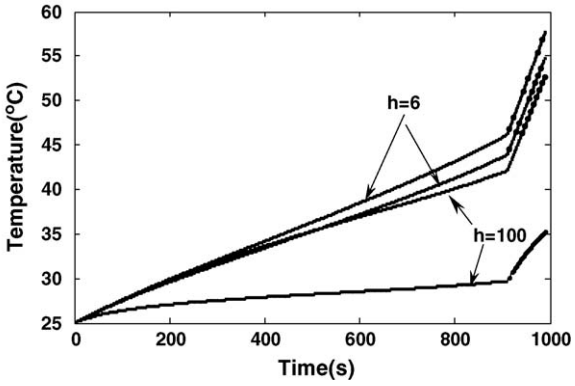

Fig. 7. Effect of heat-transfer coefficients on maximum and minimum temperature under 4C charge.

When approaching the overcharge region, the difference between maximum and minimum temperature increases dramatically with a higher heat-transfer coefficient. When the heat-transfer coefficient equals $6\,W\,m^{-2}\,K^{-1}$, the difference between maximum and minimum temperature across the battery is only about $3\,^{\circ}C$ at the end of 4C charge, while the heat transfer coefficient increases up to $100\,Wm^{-2}\,K^{-1}$, the value is remarkably up to about $15\,^{\circ}C$ at the same condition. Non-uniformed temperature profiles result in different electrochemical behaviors, and in turn, cause the battery performance fade. Together with Fig. 6, it is shown that the only increase of the heat transfer coefficient cannot efficiently improve the uniformity of temperature across the whole battery in spite of a lower average temperature the system can obtain. It can also be seen that the worse results encounter when overcharged, the temperature differences trend to larger values when the heat-transfer coefficients increase.

4.5. Effect of heat conductivities on temperature profile

The heat conductivity is decided by the battery structure, electrode structures and materials. According to Ref. [9], heat conductivity is related to the electrode porosity and the ratio of positive, negative electrode and separator, which decide the electrochemistry of battery system; therefore, it is not practical to change the heat conductivity in large scale for the actual battery. To study the effect of heat conductivities on battery thermal behavior, an assumption with a small change range of heat conductivity was adopted in this work. Fig. 8 compared the effect of different heat conductivity on the battery temperature profile in r-direction. It can be seen that the maximum temperature decreases and minimum temperature increases with the increase in thermal conductivity in r-direction. When λ_r rise about 30% from 0.74 to $0.96\,W\,m^{-1}\,K^{-1}$, although the battery temperature decreases slightly, the temperature profile becomes more uniform, the difference between the maximum and minimum temperature across the battery decreases from 3.5 to $2.7\,^{\circ}C$, while λ_r drops about 30% from 0.74 to $0.56\,W\,m^{-1}\,K^{-1}$, the battery temperature increases slightly, but the temperature profiles become

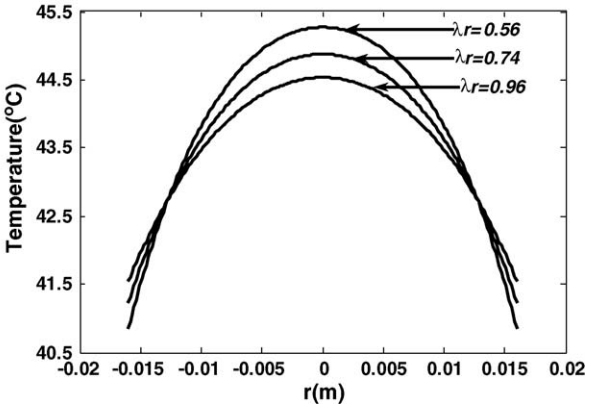

Fig. 8. Temperature profiles under different conductivities in r-direction ($z = H/2$) at the charge end of 4C rate ($\lambda_z = 0.84\ \mathrm{W\,m^{-1}\,K^{-1}}$, $T_0 = 25\ ^\circ\mathrm{C}$).

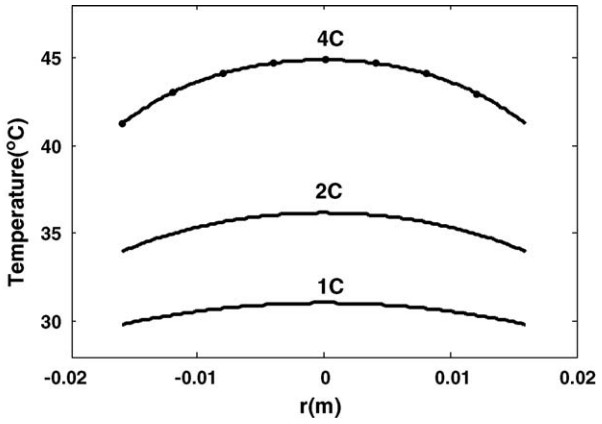

Fig. 9. Temperature profile in the battery ($z = H/2$) in r-direction under different charge rates ($\lambda_r = 0.74\ \mathrm{W\,m^{-1}\,K^{-1}}$, $\lambda_z = 0.84\ \mathrm{W\,m^{-1}\,K^{-1}}$, $T_0 = 25\ ^\circ\mathrm{C}$, $h = 25\ \mathrm{W\,m^{-2}\,K^{-1}}$).

more non-uniformed, the difference between the maximum and minimum temperature across the battery rises from 3.5 to 4.6 °C. It seems that the increase of thermal conductivity can obtain a more uniformed temperature profile based on the thermal modeling. In general, the increase of the heat conductivity can improve the uniformity of battery temperature profile to some extend in the actual battery, but this leads probably to the battery electrochemistry changes which contradict to the improvement of heat conductivities. However, from a heat transport point of view, some better designs could be achieved by which temperature gradient within a battery is minimized [5].

4.6. Effect of charging rates on temperature profiles

Fig. 9 shows temperature profiles of an 8-Ah Ni/MH battery in r-direction ($z = H/2$) under different charge rates. It can be seen that under low charge rate, the temperature in the battery presents a small increase, however, under high charge rates, the temperature rise in the battery is very high. The maximum temperature in the battery rises from 25 to 31, 36 and 45 °C at the end of 1C, 2C and 4C charge, respectively. Furthermore, when charge rates increase, the temperature gradients of the battery become steeper under the same condition. The difference between maximum and minimum temperature rises from 0 to 3, 5 and 7 °C at the end of 1C, 2C and 4C charge, respectively. The similar results can be obtained in z-direction. The calculated results indicate that a higher charge rate leads to a higher temperature rise and a less uniformed temperature profile, which are harmful to the battery performance. Obviously, a more efficient heat removal should be selected in order to adopt higher charge rates, which results in much faster heat generation rate.

4.7. Effect of overcharge on temperature profiles

Fig. 10 shows the effect of overcharge on the temperature profiles of the battery. It can be seen that the overcharge results in a serious temperature rise and a less uniformed temperature profile. Almost all the current applied to the battery is used to generate oxygen at the positive electrode during overcharge. The generated oxygen at the positive electrode can be reduced at the negative electrode, and this reduction reaction will generate much more heat than that from battery internal resistance, and hence a steeper temperature rise.

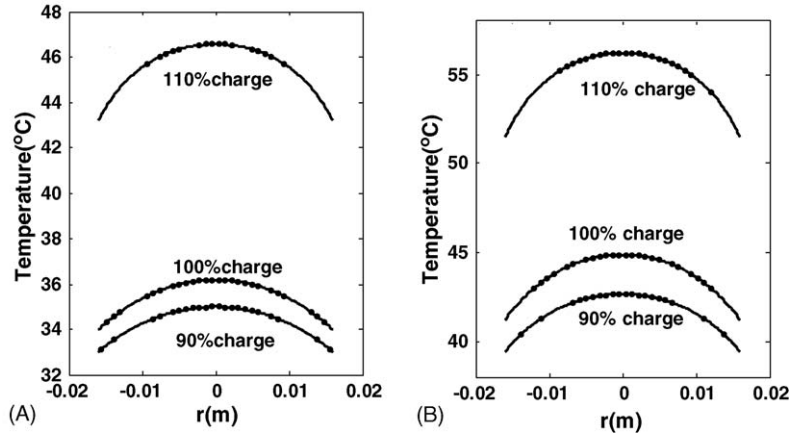

Fig. 10. Effect of overcharge on the temperature profiles in r-direction at the charge end of 2C rate (A) and 4C rate (B).

When input charge rises 10% from 90% to 100% of nominal capacity, the maximum temperature rises only 1 and 2 °C under 2*C* and 4*C* charge, respectively, while input charge rises 10% from 100% to 110% of nominal capacity, the maximum temperature increasingly rises 10 and 12 °C under 2*C* and 4*C* rates overcharge, respectively. The difference between maximum and minimum temperature is 5 and 7 °C at 100% charge input under 2*C* and 4*C* rate charge, respectively, while the difference rises even up to 7 and 9 °C at 10% overcharge under 2*C* and 4*C* rates, respectively. Obviously, overcharge leads to overheat and hence a stronger temperature rise and a steeper temperature gradient. Therefore, overheat can lead to a violent change of battery electrochemistry, which will result in dangerous situation. Overcharge modeling can give some important information of system temperature variations when charge-control system fails. The calculation indicates that it is necessary to avoid overcharge when fast charging the Ni/MH battery.

5. Conclusions

Thermal analysis of cylindrical nickel-metal hydride batteries during fast charge has been carried out by the two-dimensional thermal modeling proposed in this work. Detailed information, such as effects of dissipating heat coefficient, heat conductivity, charge rate and overcharge on the battery temperature profile across the battery during fast charge can be digitally obtained. The thermal behavior of batteries can be better understood with these simulated results from the mathematical modeling. Based on the results obtained from model calculation and experimental measurements, it can be seen that the increase of the heat-dissipating coefficient can decrease the battery temperature, but leading to a less uniformed temperature profile across the whole battery. A more uniformed temperature profile can be obtained when adopting a large heat conductivity, which may probably be achieved by improving the battery electrode structure and materials. When charge rates increase the battery temperature increasingly rises and the temperature profiles become less uniformed under the same input charge, overcharge results in a dangerous temperature rise, which should be avoided carefully.

Acknowledgments

This work was supported by the *National Key Basic Research and Development Program of China* (grant no. 2002CB211800), and *the National EV(863)key Program of China* (grant no. 2003AA501231).The authors are grateful to Prof. Cun-Mao Hong of Peking University for his knowledgeable comments on this work, and Mr. Dao-Zhong Hu for his assistance in the experimental work.

References

[1] P.M. Gomadam, Electrochemical–thermal modeling of lithium-ion batteries, Ph.D. Thesis, UMI, MI, 2003.
[2] Y. Chen, J.W. Evans, J. Electrochem. Soc. 143 (1996) 2708.
[3] X.-G. Yang, B.Y. Liaw, J. Electrochem. Soc. 151 (2004) 265.
[4] W.B. Gu, C.Y. Wang, J. Electrochem. Soc. 147 (2000) 2910.
[5] Y. Chen, J.W. Evans, Electrochim. Acta 39 (1994) 517.
[6] T.L. Evans, R.E. White, J. Electrochem. Soc. 136 (1989) 2145.
[7] E.E. Kulu, R.E. White, J. Electrochem. Soc 140 (1993) 23.
[8] M.S. Wu, Y.H. Hung, Y.Y. Wang, C.C. Wan, J. Electrochem. Soc. 147 (2000) 930.
[9] M.S. Wu, Y.Y. Wang, C.C. Wan, J. Power Sources 74 (1998) 202.
[10] D. Bernardi, E. Pawlikowski, J. Newman, J. Electrochem. Soc. 132 (1985) 5.
[11] N. Sato, K. Yagi, JASE Rev. 21 (2000) 205.
[12] S.A. Hallaj, H. Maleki, J.S. Hong, J.R. Selman, J. Power Sources 83 (1999) 1.
[13] L. Rao, J. Newman, J. Electrochem. Soc. 144 (1997) 2796.
[14] D. Berndt, Maintenance-Free Batteries, Wiley, New York, 1993.
[15] J. Kim, T.V. Nguen, R.E. White, J. Electrochem. Soc. 139 (1992) 2781.